

## A Red Giants' Toy Story II: Understanding the Red-Giant Branch Bump

MARCELO M. MILLER BERTOLAMI<sup>1,2</sup>

<sup>1</sup>*Instituto de Astrofísica de La Plata, Consejo Nacional de Investigaciones Científicas y Técnicas  
Avenida Centenario (Paseo del Bosque) S/N, B1900FWA La Plata, Argentina.*

<sup>2</sup>*Facultad de Ciencias Astronómicas y Geofísicas, Universidad Nacional de La Plata  
Avenida Centenario (Paseo del Bosque) S/N, B1900FWA La Plata, Argentina.*

(Received February 29, 2021; Revised February 30, 2022; Accepted February 31, 2023)

Submitted to ApJ

### ABSTRACT

The Red-Giant Branch Bump (RGBB) is one of the most noteworthy features in the red-giant luminosity function of stellar clusters. It is caused by the passage of the hydrogen-burning shell through the composition discontinuity left at the point of the deepest penetration by the convective envelope. When crossing the discontinuity the usual trend in increasing luminosity reverses for a short time before it increases again, causing a zig-zag in the evolutionary track.

In spite of its apparent simplicity the actual physical reason behind the decrease in luminosity is not well understood and several different explanations have been offered.

Here we use a recently proposed simple toy-model for the structure of low-mass red giants, together with previous results, to show beyond reasonable doubt that the change in luminosity at the RGBB can be traced to the change in the mean molecular weight of the layers on top of the burning shell. And that these changes happen on a nuclear timescale. The change in the effective mean molecular weight, as the burning shell approaches the discontinuity, causes a drop in the temperature of the burning shell which is attenuated by the consequent feedback contraction of the layers immediately below the burning shell.

Our work shows that, when applied correctly, including the feedback on the structure of the core together with of the increase in the mass of the core, shell-source homology relations do a great quantitative job in explaining the properties of full evolutionary models at the RGBB.

*Keywords:* Stellar structures — Stellar Evolution — Giant Branch — Stellar Interiors

### 1. INTRODUCTION

It was discovered already in the early days of automatic stellar evolution computations that low-mass stars undergo a brief phase of decreasing luminosity (Thomas 1967; Iben 1968) during the red giant branch (RGB). This drop in luminosity is caused by the passage of the hydrogen(H)-burning shell through the composition discontinuity left by the deepest penetration of convection into the stellar envelope (Fig 1). This creates a zig-zag in the evolutionary track, and the star crosses the same luminosity region three times. Consequently,

red giants spend a little longer in that region of the Hertzsprung–Russell (HR) diagram. In stellar clusters this phase corresponds to an accumulation of stars at that specific luminosity. This produces a bump in the luminosity function of red giant branch stars that was first measured by King et al. (1985), and it is usually known as the red-giant branch bump (RGBB).

In spite of its apparent simplicity the actual physical mechanism behind the sudden decrease in luminosity is not well understood. Iben (1968) suggested that the drop in the stellar luminosity was a direct effect of the increase in the abundance of H in the burning shell when crossing the chemical discontinuity. Despite the absence of a clear mechanism for this connection several other authors have concurred with this position (e.g. Cassisi et al. 2002; Gai & Tang 2015). Neverthe-

less, a detailed analysis of stellar models around the RGBB by Sweigart et al. (1990) showed that luminosity starts dropping before the hydrogen-burning shell actually reaches the hydrogen discontinuity. They concluded that the luminosity drop cannot be due to the burning shell responding to the increase in the available fuel, as that fuel has not yet been reached. Instead, they suggested that the drop in luminosity should be due to the increase in the opacity above the burning shell that results from the higher H abundance. Taking a completely different approach Hekker et al. (2020) analyzed the temporal changes in the entropy distribution during the drop in luminosity at the RGBB. A more likely explanation of the RGBB was suggested by Refsdal & Weigert (1970) who, under the assumption of the so called shell-source homology relations (see appendix A), noticed that the drop in the mean molecular weight ( $\mu$ ) at the transition should cause a drop in the luminosity of the burning shell. This idea was further explored by Christensen-Dalsgaard (2015) who studied in detail the impact of variations of  $\mu$  in the layers immediately above the burning shell. Christensen-Dalsgaard (2015) concluded that it is plausible that the mean molecular weight above the burning shell is the main cause of the drop in luminosity. The main problem with this explanation, as noted by Christensen-Dalsgaard (2015), is the substantial departure in the predictions of shell-source homology relations from those of full evolutionary models (FEMs), which calls into question the validity of the argument.

Recently, we have developed a simple solution the long standing question of why stars become red giants (Miller Bertolami 2022). As part of this explanation we devised a quantitative toy-model for low-mass red giants (Fig. 2). One of the key insights from this model is that the location of the burning shell ( $R_s$ ) is not independent from the temperature of the shell ( $T_s$ ). Consequently, when the burning shell approaches the chemical discontinuity the decrease in  $\mu$  immediately above the burning shell leads to a drop in temperature in the isothermal layer between the degenerate core and the burning shell (see Fig 2). As this isothermal region has the equation of state of an ideal classical gas, this cooling leads to a contraction. According to shell-source homology relations, this feedback of the temperature drop on the location of the burning shell should also affect the luminosity of the burning shell. In this paper we show how the feedback of the radius of the burning shell leads to a very good agreement between the predictions of the simple model and those of FEMs, proving beyond reasonable doubt that it is the change in  $\mu$  what causes the RGBB.

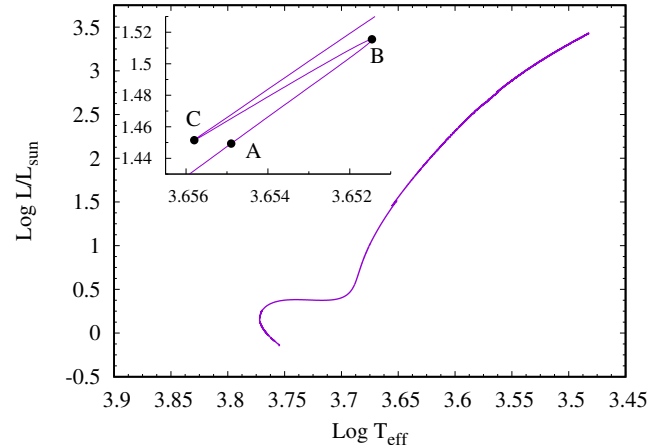


**Figure 1.** Evolutionary track of a  $1M_{\odot}$  model (initial composition  $X = 0.695$  and  $X = 0.02$ ). Inset: Zoom in the region of the RGBB. Letters A, B and C indicate the location of the models snapshots discussed in the text.

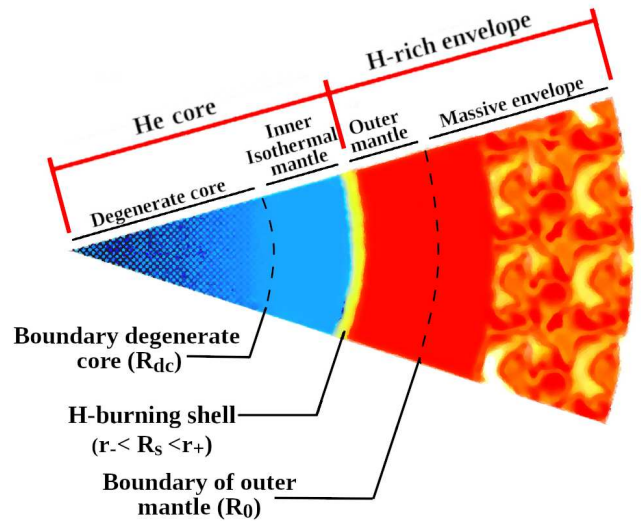


**Figure 2.** Main structural parts and definitions of low-mass red giants and the toy model developed in Miller Bertolami (2022). The inner and outer mantles around the burning shell are, in most cases, nondegenerate and massless.

## 2. DEFINITIONS, SHELL-SOURCE HOMLOGY RELATIONS AND SIMPLE MODELS

For the sake of clarity we will first define some relevant quantities. Following Miller Bertolami (2022) the structure of a low-mass red giant can be described as consisting of a degenerate core of mass ( $M_c$ ) and radius ( $R_{dc}$ ) surrounded by a massless isothermal mantle where the gas behaves as an ideal classical gas. Above sits the H-burning shell, where heat is being released by nuclear burning. We define  $r_-$  and  $r_+$  as the lower and upper boundaries of the burning shell, where the local luminosity ( $l(r)$ ) goes from the value at the core ( $L_c$ ) to

the surface value  $L_\star = L_c + L_s$ , where  $L_s$  is the total power released by the burning shell. Due to degeneracy of the electron gas, the core contracts only due to the increase in its mass, which happens on a nuclear timescale making the heat released by gravitational contraction  $L_c \ll L_s \simeq L_\star$ . We define the nominal location of the burning shell ( $R_s$ ) as the point at which  $l(R_s) \simeq L_s/2$ , which is very close to the maximum in the energy generation rate. Thanks to the high temperature sensitivity of nuclear reactions the burning shell can be assumed to be thin,  $|r_+ - r_-| \ll R_s$ . Under this assumption  $R_s$  is also the radius of the helium (He) core. Above the burning shell it is useful to define an outer mantle between  $r_+$  and an arbitrary point  $R_0$  at which pressure, temperature and density have dropped by orders of magnitude from their values at the burning shell ( $P_0 \ll P_s$ ,  $T_0 \ll T_s$ ,  $\rho_0 \ll \rho_s$ ). Let us note that above  $r_+$  already  $l(r) = L_\star \simeq L_s$  and the composition is that of the hydrogen rich envelope (corresponding to a mean molecular weight  $\mu_{\text{env}}$ ). As discussed in Miller Bertolami (2022) as soon as the core is dense ( $\rho_s \ll 4\pi M_c/3R_s^3$ ) the outer mantle can be considered massless  $\Delta m \ll M_c$ .

One usual way of understanding the behavior of burning shells is with the help of the so-called shell-source homology relations developed by (Refsdal & Weigert 1970). Shell-source homology rests on several assumptions (see appendix A), in particular it is assumed that the region between  $r_-$  and  $R_0$  is massless ( $\Delta m \ll M_c$ ), and that the solutions  $\rho(r)$ ,  $T(r)$ ,  $P(r)$ , and  $l(r)$  of the stellar structure equations only depend on  $M_c$ ,  $R_s$  and the mean molecular weight ( $\mu$ ) through simple power laws. Under these assumptions it is possible to show that two different solutions  $\rho(r)$ ,  $T(r)$ ,  $P(r)$ ,  $l(r)$  (corresponding to  $M_c, R_s$ , and  $\mu$ ), and  $\rho'(r')$ ,  $T'(r')$ ,  $P'(r')$ ,  $l'(r')$  (corresponding to  $M'_c, R'_s$ , and  $\mu'$ ) evaluated at homologous points ( $r/R_s = r'/R'_s$ ) are related by

$$\frac{\rho}{\rho'} = \left(\frac{M_c}{M'_c}\right)^{(4-\nu)/3} \left(\frac{R_s}{R'_s}\right)^{(-6+\nu)/3} \left(\frac{\mu}{\mu'}\right)^{(4-\nu)/3} \quad (1)$$

$$\frac{T}{T'} = \left(\frac{M_c}{M'_c}\right) \left(\frac{R_s}{R'_s}\right)^{-1} \left(\frac{\mu}{\mu'}\right) \quad (2)$$

$$\frac{P}{P'} = \left(\frac{M_c}{M'_c}\right)^{(7-\nu)/3} \left(\frac{R_s}{R'_s}\right)^{(-9+\nu)/3} \left(\frac{\mu}{\mu'}\right)^{(4-\nu)/3} \quad (3)$$

$$\frac{l}{l'} = \left(\frac{M_c}{M'_c}\right)^{(8+\nu)/3} \left(\frac{R_s}{R'_s}\right)^{(-3-\nu)/3} \left(\frac{\mu}{\mu'}\right)^{(8+\nu)/3}, \quad (4)$$

where we have used a Thomson scattering opacity ( $\kappa = \kappa_0 T^a P^b = \kappa_0$ , i.e.  $a = b = 0$ ) and a typical CNO energy generation rate ( $\epsilon = \epsilon_0 \rho T^\nu$ ). It is also worth noting that, as  $\mu(r)$  changes in the region of the burning shell, to obtain eqs. 1 to 4 one needs to assume that  $\mu'(r'/R'_s)$  can be obtained by scaling up the func-

tion  $\mu(r/R_s)$  by the same factor at each homologous point. This is clearly not completely accurate, as the value at the bottom of the burning shell ( $r = r_-$ ) in FEMs has to remain constant and equal to the mean molecular weight of the core ( $\mu_- = \mu'_- = \mu_c$ ). Alternatively, the values of  $\mu$  and  $\mu'$  can be understood, within the framework of shell-source homology relations as a proper average of the mean molecular weight in relevant region (see Refsdal & Weigert 1970, for a discussion).

Interestingly in Miller Bertolami (2022) we have shown that, when the core is dense enough it is possible to prove that the values of  $\rho_s$ ,  $T_s$ ,  $P_s$  in the middle of the burning shell, and the total luminosity  $L_s$  of the burning shell are only dependent on the values of  $M_c$  and  $R_s$  as assumed in shell-source homology relations. Moreover, it is possible to show that these quantities fulfill relationships similar to eqs. 1 to 4. Under the assumption of an inert core ( $L_c = 0$ ), Thomson scattering, and a typical CNO energy generation rate eqs. 32, 35, 36 and 37 of Miller Bertolami (2022) tell us that

$$\rho_s = \mathcal{K} M_c^{(4-\nu)/3} R_s^{(-6+\nu)/3} \mu_{\text{env}}^{(2-\nu)/3} \mu_s^{2/3} \quad (5)$$

$$T_s = \mathcal{K}' M_c R_s^{-1} \mu_{\text{env}} \quad (6)$$

$$P_s = \mathcal{K}'' M_c^{(7-\nu)/3} R_s^{(-9+\nu)/3} \mu_{\text{env}}^{(5-\nu)/3} \mu_s^{-1/3} \quad (7)$$

$$L_s = \mathcal{K}''' M_c^{(8+\nu)/3} R_s^{(-3-\nu)/3} \mu_{\text{env}}^{(7+\nu)/3} \mu_s^{1/3}, \quad (8)$$

where  $\mathcal{K}$ ,  $\mathcal{K}'$ ,  $\mathcal{K}''$ ,  $\mathcal{K}'''$  are constants,  $\mu_s$  is the mean molecular weight at the middle of the burning shell and  $\mu_{\text{env}}$  is the mean molecular weight of the envelope (assumed to be constant in the outer mantle). By comparing eqs. 1 to 4 and eqs. 5 to 8 we see that under the assumption performed in the derivation of shell-source homology relations, that changes in  $\mu_s$  are proportional to changes in  $\mu_{\text{env}}$ , the two sets of relations are formally similar. It is worth noting that, under the framework provided by Miller Bertolami (2022) the quantities in eqs. 5 to 8 correspond to the values of  $\rho(r)$ ,  $T(r)$ ,  $P(r)$ ,  $l(r)$  at specific points and the meaning of the mean molecular weights are now well defined. Due to the large value of  $\nu$  it is clear from eqs. 5 to 8 that it is  $\mu_{\text{env}}$  what dominates the impact of changes in the molecular weight on the burning shell. This should not be a surprise, as it is only  $\mu_{\text{env}}$  what links  $T_s$  to  $M_c$  and  $R_s$  and nuclear burning is extremely sensitive to temperature. For the sake of clarity, in the following discussion we will assume that  $\Delta\mu_s/\mu_s = \Delta\mu_{\text{env}}/\mu_{\text{env}}$  as usually done in shell-source homology relations. In real stars it is expectable that relative changes in  $\mu_s$  will be between  $\Delta\mu_{\text{env}}/\mu_{\text{env}}$  and  $\Delta\mu_-/\mu_- = 0$ . Interestingly, due to the large value of  $\nu$  this will be only a minor correction.

Miller Bertolami (2022) showed that the core of a low-mass red giant can be considered to good approximation

as composed of two parts, a degenerate core of mass  $M \simeq M_c$  and radius  $R_{dc} \simeq 1.12 \times 10^{20} M_{dc}^{-1/3}$ . and an inner nondegenerate isothermal mantle of negligible mass above (see Fig. 2). It is possible to show that the temperature, density, pressure and radius of the burning shell, and the mass of the core and mean molecular weight at and above the burning shell are not independent but must fulfill

$$T_9 \simeq \frac{\mu_{env}}{\mu_c} 0.6 \frac{R_{dc}}{R_s} \left( \frac{M_c}{M_\odot} \right)^{4/3}, \quad (9)$$

and

$$\begin{aligned} & 1.633 \times 10^{-26} \frac{\mu_c^3}{\mu_s \mu_{env}^2} \nu \exp(21/\nu) (1 + 1/\nu)^{-9/2} \\ & = T_9^{-1/6} \left[ \frac{R_s}{R_{dc}} \right]^2 \left[ \frac{M_c}{M_\odot} \right]^{-2/3} \\ & \times \exp \left[ \frac{12}{(1 + 2/\nu)} \frac{\mu_c}{\mu_{env}} \left( 1 - \frac{R_s}{R_{dc}} \right) \right. \\ & \left. - 15.231 T_9^{-1/3} \right] \end{aligned} \quad (10)$$

where  $T_9 = T_s/10^9$  as it is common practice, and  $R_{dc}$  is the radius of the degenerate part of the He core (see Fig. 2). Eqs. 9 and 10 have been derived for the CNO-cycle and Thomson scattering opacities.

### 3. UNDERSTANDING THE RGBB

Table 1 shows the characteristics of the stellar models before and after the RGBB (Figs. 3 and 4). One of the characteristics of the models near the RGBB is the presence of the chemical discontinuity at  $m_{dis} \simeq 0.242 M_\odot$  ( $r = R_{dis}$ ) which was left by the maximum penetration of the convective envelope at earlier evolutionary stages. From Table 1 we see that the relative drop in luminosity at the RGBB (from B to C) for our reference model is  $\delta L_\star/L_\star = (L_C - L_B)/L_B = -0.1372$ , while the relative drop in the mean molecular weight<sup>1</sup> is  $(\mu_C - \mu_B)/\mu_B = -0.1126$ . It is clear that the drop in luminosity is much lower than what would be predicted from a naive use of the shell-source homology relations (e.g. Refsdal & Weigert 1970; Kippenhahn et al. 2012). For Thomson scattering, which is a good approximation of the opacity at the burning shell, and the typical assumption of  $\nu = 13$  (Kippenhahn et al. 2012)<sup>2</sup>

<sup>1</sup> Here the value of the mean molecular weight is taken immediately above the burning shell ( $r \simeq r_+$ ), where the energy generation rate falls two orders of magnitude below the peak value.

<sup>2</sup> As we mention in appendix A at the typical temperatures of the RGBB ( $T_s \simeq 2.85 \times 10^7$  K) the temperature dependence of the CNO cycle is closer to  $\nu = 16$ . For the sake of comparison with previous works we keep  $\nu = 13$  in this estimations.

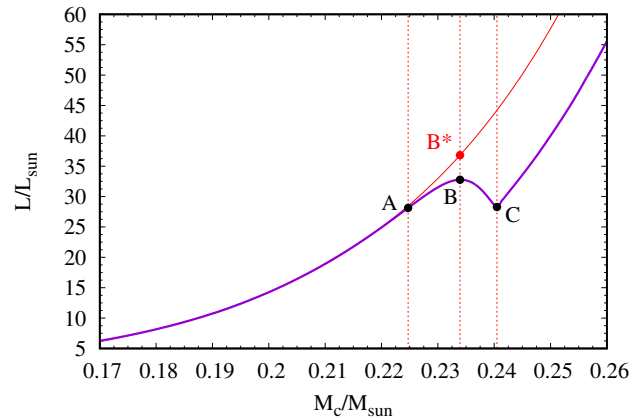


**Figure 3.** The purple line shows the evolution of the luminosity as a function of the mass of the core for the FEM shown in Fig. 1. The red line shows an extrapolation of the evolution of  $L(M_c)$  before point A, where the effect of the chemical discontinuity on the outer mantle is still not important. The difference between the red and purple lines is, then, a measure of the impact of the chemical discontinuity on  $L(M_c)$ .

the dependence of the luminosity on the mean molecular weight predicted by shell-source homology relations (eqs. 1 to 4) is  $L_s \propto \mu^7$ . For the change in  $\mu_+$  in the outer mantle between model B and C (see Table 1), this predicts  $\delta L_s/L_s = 7 \times \delta\mu/\mu = -0.7882$ . We see that a naive use of the shell-source homology relations manages to predict the right trend in luminosity but errs by more than a factor 5.7. The difference is still unacceptable if we choose the value of  $\mu$  immediately below the discontinuity,  $\mu_{dis-}^B = 0.7066$ , which gives  $\delta\mu/\mu = -0.1053$  and  $\delta L_s/L_s = -0.7371$  (a factor 5.4 larger than observed in the models).

We will show below the agreement is improved by more than an order of magnitude when shell-source homology relations are applied in a more nuanced way.

#### 3.1. An improvement: the effective mean molecular weight of the outer mantle

Christensen-Dalsgaard (2015) studied in detail the impact of variations of  $\mu$  in the layers immediately above the burning shell. Christensen-Dalsgaard (2015) noted that, when the burning shell approaches the discontinuity in the H profile, the relevant molecular weight ( $\mu_{eff}$ ) that links  $T_s$ ,  $R_s$  and  $M_c$ ,

$$T_s \simeq \frac{G M_c \mu_{eff}}{R_s \Re} \nabla_+, \quad (11)$$

is a mixture of the molecular weight above ( $\mu_\uparrow$ ) and below ( $\mu_\downarrow$ ) the discontinuity ( $\nabla_+ = 1/4$  for Thomson scattering). He showed that the effective molecular weight

Snapshot	$M_c/M_\odot$	$L_*/L_\odot$	$R_s$ [cm]	$R_{\text{dis}}$ [cm]	$T_s$ [ $10^7$ K]	$\rho_s$ [g cm $^{-3}$ ]	$\mu_+$	$\mu_{\text{eff}}$
model A	0.226146	28.1423	$2.1900 \times 10^9$	$2.1164 \times 10^{10}$	2.8515	149.54	0.7212	0.7120
model B	0.235181	32.7756	$2.1477 \times 10^9$	$7.2146 \times 10^9$	2.9055	144.58	0.7124	0.6885
model C	0.241617	28.2800	$2.0636 \times 10^9$	-	2.8741	158.08	0.6322	0.6322

**Table 1.** Properties of the structure of the stellar model at the snapshots displayed in Fig. 3 ( $1M_\odot$  ( $Z = 0.02$ ) sequence). The value  $\mu_+$  is taken immediately above the burning shell ( $r \simeq r_+$ ).

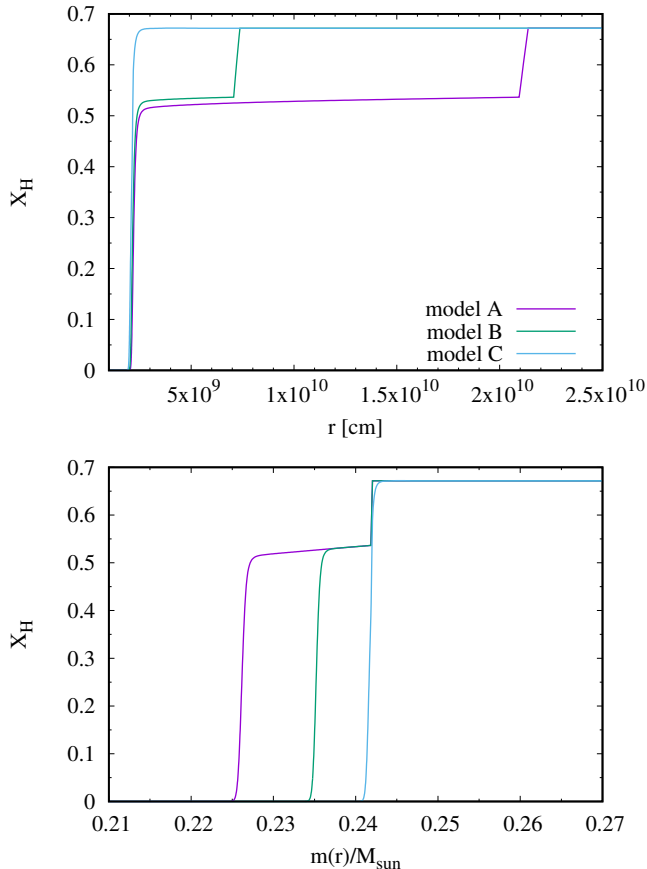


**Figure 4.** Radial chemical profiles of the FEMs at different stages near the RGBB (see Figs. 1 and 3). The chemical discontinuity left by the maximum penetration of the convective envelope at earlier evolutionary stages can be clearly appreciated at  $m(r) \simeq 0.242M_\odot$ .

felt by the burning shell can be written as

$$\mu_{\text{eff}} = \mu_\downarrow \left[ 1 - \frac{R_s}{R_{\text{dis}}} \left( 1 - \frac{\mu_\uparrow}{\mu_\downarrow} \right) \right]. \quad (12)$$

Eq. 11 is, in fact, eq. 6 and it is the reason why  $\mu_{\text{env}}$  appears in all the other equalities. This implies that, as the burning shell approaches the discontinuity in the chemical profile, it is  $\mu_{\text{eff}}$  what plays the role of  $\mu_{\text{env}}$  in eqs. 5 to 8. Note that Eq. 12 was derived for a idealized situation where the mean molecular weight is strictly constant between the burning shell and the discontinuity which is not the case in real stars

(Fig.4). When estimating  $\mu_{\text{eff}}$  in FEMs we use  $\mu_\downarrow \simeq \mu_+$ . Using these expressions, we see that the mean molecular weight actually felt by the burning shell before reaching the discontinuity is slightly lower. The values for each snapshot are shown in the last column of Table 1. With the corrected values we now see that, from B to C, the drop in the effective mean molecular weight is  $\delta\mu_{\text{eff}}/\mu_{\text{eff}} = -0.0818$ . Again, with the assumption of Thomson scattering and  $\nu = 13$ , we have that  $L_s \propto \mu_{\text{eff}}^7$ , this would imply  $\delta L/L = -0.5724$ , which is still a factor 4.2 higher than the actual value. As noted by Christensen-Dalsgaard (2015) while this correction to the mean molecular weight improves the agreement with the drop in luminosity observed in FEMs, the disagreement is still substantial. This disagreement suggest some missing ingredients.

Interestingly, one of the missing ingredients becomes evident when looking at the evolution of luminosity as a function of the mass of the core (see Fig. 3). Within this picture, the impact of the chemical discontinuity happens as the core grows and the burning shell approaches the discontinuity. Then, it is not completely correct to neglect the increase in the core mass as the luminosity drops. From B to C the core mass changes by  $\delta M_c/M_c = 0.027366$ . Recalling that for  $\nu = 13$  (eqs. 1 to 4) now  $L_s \propto M_c^7 \mu_{\text{eff}}^7$  this decreases the shell homology prediction of the luminosity drop to  $\delta L/L = -0.3804$ . This is still a factor 2.8 difference from that observed in FEMs (a  $\sim 180\%$  difference in  $\delta L_s/L_s$ ), but a significant improvement over the naive estimation.

We show in the next section that the final key missing ingredient comes from the feedback of the changes in the shell temperature on the inner mantle (the isothermal mantle below the burning shell).

### 3.2. The feedback on the inner mantle

As summarized in the appendix A, shell-source homology relations predict that the luminosity of the burning shell depends on  $M_c$ ,  $R_s$ , and  $\mu$ . For a typical Thomson scattering opacity law, and  $\nu = 13$ , this dependence is as

$$L_s \propto M_c^7 R_s^{-16/3} \mu_{\text{env}}^7, \quad (13)$$

or

$$\frac{\delta L_s}{L_s} = 7 \frac{\delta M_c}{M_c} - \frac{16}{3} \frac{\delta R_s}{R_s} + 7 \frac{\delta \mu_{\text{env}}}{\mu_{\text{env}}}. \quad (14)$$



Interestingly, as clarified by eqs. 9 and 10 a change in the mean molecular weight of the outer mantle ( $\mu_{\text{env}}$ ), in a model of given core mass ( $M_c$ ), will affect the radius of the burning shell ( $R_s$ ). This is because, any drop (increase) in the temperature of the shell leads to a drop (increase) in the temperature of the ideal gas layers immediately below the burning shell, with the consequent contraction (expansion) of those layers. Interestingly, a drop in the radius of the burning shell will lead to higher temperatures than if the radius were to stay fixed.

We can determine from eqs. 9 and 10 how changes in  $\mu_{\text{env}}$  and  $R_s$  are connected for the typical core masses at which the RGBB takes place. Assuming, as before, that  $\mu_s \propto \mu_{\text{env}}$ , eq. 10 can be written as

$$\begin{aligned} C \simeq T_9^{-1/6} \left[ \frac{\mu_{\text{env}}}{\mu_c} \right]^3 \left[ \frac{R_s}{R_{dc}} \right]^2 \left[ \frac{M_c}{M_\odot} \right]^{-2/3} \\ \times \exp \left[ 10.4 \frac{\mu_c}{\mu_{\text{env}}} \left( 1 - \frac{R_s}{R_{dc}} \right) - 15.231 T_9^{-1/3} \right], \end{aligned} \quad (15)$$

where we have used that  $\nu = 13$  as before. Calling  $x = R_s/R_{dc}$ ,  $z = \mu_{\text{env}}/\mu_c$  and  $m = M_c/M_\odot$  it is easy to show from eqs. 9 and 15 that, for a constant mass of the core<sup>3</sup> we have

$$\begin{aligned} 0 \simeq \frac{17}{6} \frac{\delta z}{z} + \frac{13}{6} \frac{\delta x}{x} - 10.4(1-x) \frac{\delta z}{z^2} - 10.4 \frac{\delta x}{z} \\ - (18.058 m^{-4/9}) \times \left[ \frac{z^{-1/3} x^{-2/3}}{3} \delta x - \frac{z^{-4/3} x^{1/3}}{3} \delta z \right]. \end{aligned} \quad (16)$$

Replacing the typical values of  $m$ ,  $x$  and  $z$  for the stellar structure near the RGBB,  $m \approx 0.2384$ ,  $x \approx 1.495$ , and  $z \approx 0.53$  we find that

$$\frac{\delta R_s}{R_s} \simeq 0.66 \frac{\delta \mu_{\text{env}}}{\mu_{\text{env}}}. \quad (17)$$

Had we assumed that  $\mu_s$  remained unchanged while  $\mu_{\text{env}}$  changed, then the proportionality constant in eq. 17 would have been 0.64. Similarly, had we assumed a value of  $\nu = 16$ , the constant in eq. 17 would have remained basically unchanged at 0.66. Eq. 17 is key to understand the luminosity drop at the RGBB. Eq. 17 tells us that a drop in the mean molecular weight will create a similar drop in the radius of the burning shell. This  $\delta R_s$  will act to increase the temperature and attenuate the impact of  $\delta \mu_{\text{env}}$  on the luminosity of the burning shell. As discussed in Section 3.1, when there is a chemical discontinuity in the outer mantle,  $\mu_{\text{env}}$  in the previous equations must be replaced by  $\mu_{\text{eff}}$  (eq. 12).

If we use the result from eq. 17 in eq. 14 we see that

$$\frac{\delta L_s}{L_s} \simeq 7 \frac{\delta M_c}{M_c} + 3.48 \frac{\delta \mu_{\text{eff}}}{\mu_{\text{eff}}}, \quad (18)$$

<sup>3</sup> This means that also  $R_{dc}$  can be considered constant.

where it becomes clear how the feedback in the radius of the burning shell effectively decreases the impact of the change in the mean molecular weight.

If we now we use eq. 18 to assess the drop in luminosity from model B to model C ( $\delta M_c/M_c = 0.027366$  and  $\delta \mu_{\text{eff}}/\mu_{\text{eff}} = -0.0818$ ), we get  $\delta L/L \simeq -0.093$  which is only 32% less than the actual value observed in the FEM. This small difference is a huge improvement over the differences obtained in the previous sections, when the feedback of the core was neglected.

We see that, when the feedback of the inner mantle is included in our estimations of the luminosity drop, shell-source homology relations do a remarkable job in explaining the observed luminosity drop at the RGBB. Moreover, we can now use these results to understand why the luminosity increase slows down from model A to model B (see Fig. 3). From Table 1 we see that, from model A to model B the core increases by  $\delta M_c/M_c \simeq 0.04$ . In the absence of any other effect this would translate into an increase of the shell luminosity of  $\delta L/L \simeq 0.28$ , which is similar to the value between A and B\* in Fig. 3, but significantly higher than the increase in luminosity between A and B (see Fig. 3). However, when we take into account that the effective mean molecular weight ( $\mu_{\text{eff}}$ , eq. 12) decreases as the burning shell gets closer to the discontinuity by  $\delta \mu_{\text{eff}}/\mu_{\text{eff}} \simeq -0.033$  we see that the expected change in luminosity should be  $\delta L/L \simeq 0.165$ , which is, within the quoted precision, equal to the actual luminosity change in the FEM.

We conclude that, when the feedback of changes in the shell temperature are included in the inner isothermal mantle and, consequently, in the location of the shell, shell-source homology relations do a remarkable job at explaining the luminosity changes observed on the RGBB.

#### 4. A SIMPLE DESCRIPTION OF THE RGBB

In the previous section we have shown that, by taking into account the feedback of shell temperature changes into the inner mantle and consequently the location ( $R_s$ ) of the burning shell, shell-source homology relations are able to quantitatively explain in luminosity around the RGBB. For the sake of completeness in this section we show that a very simple description of the RGBB, useful for pedagogical purposes, can be constructed with minimal assumptions.

Under the assumption that the structure of the outer mantle does not change dramatically from A to C, we can write that the mass between the burning shell and the chemical discontinuity ( $\Delta m$ ) is

$$\Delta m \simeq 4\pi R_s^2 \bar{\rho}_{UM} (R_{\text{dis}} - R_s), \quad (19)$$

where  $\bar{\rho}_{UM}$  is some mean density above the burning shell. Calling  $\delta M_c$  the increase in mass of the core since point A, we have  $\Delta m = \Delta m^0 - \delta M_c$ , where  $\Delta m^0 = M_c^C - M_c^A$ . Using this in eq. 19 we see that, at first order, we can write

$$\frac{R_{\text{dis}}}{R_s} \simeq A - B \frac{\delta M_c}{M_c} \quad (20)$$

Where the values of  $A$  and  $B$  in our model can be derived from the values on Table 1. Using eq. 20 in eq. 12 we can derive that the change in the effective mean molecular weight as the burning shell advances from A to C is

$$\frac{\delta \mu_{\text{eff}}}{\mu_{\text{eff}}} \simeq \alpha \times \left[ 1 - \frac{1}{\left(1 - \beta \frac{\delta M_c}{M_c}\right)} \right], \quad (21)$$

with  $\alpha = 0.012936$  and  $\beta = 13.1048$ . Eq. 21 captures the essence of the change in the molecular weight as the burning shell approaches the chemical discontinuity. Together with eq. 17 we see that, as the burning shell advances from model A to model C, the luminosity will follow

$$\frac{\delta L_s}{L_s} \simeq 7 \frac{\delta M_c}{M_c} + 3.48 \alpha \left[ 1 - \frac{1}{\left(1 - \beta \frac{\delta M_c}{M_c}\right)} \right]. \quad (22)$$

The evolution described by eq. 22 is shown in Fig. 5 where it is compared with the behavior of the FEM shown in Fig. 3. We see that the simple model presented in this section captures very well the behavior shown by FEMs. The main difference between the simple model and the full evolutionary structures arises from the fact that eq. 21 assumes that the mean molecular weight below the discontinuity has a constant value. As it is clear from Fig. 4 in FEMs the hydrogen profile (and consequently  $\mu$ ) has a nonzero slope. As a consequence, in FEMs as the shell approaches the discontinuity the mean molecular weight decreases faster than in our toy model due to this effect. This leads to an additional decrease in the luminosity, leading to a slightly smaller slope in the  $L_s(M_c)$  relationship. In fact, once the shell reaches the discontinuity, and the shell evolves through an homogeneous layer (after point C), the FEMs show a very similar slope to that predicted by shell-source homology relations—in particular for  $\nu = 16$  which is the correct temperature dependence of CNO burning at those temperatures.

## 5. DISCUSSION AND CONCLUSIONS

We have reanalyzed the properties of the RGBB in the light of our recent description of the properties of red giants (Miller Bertolami 2022). Specifically, we have made use of a simple description of the structure of red giants

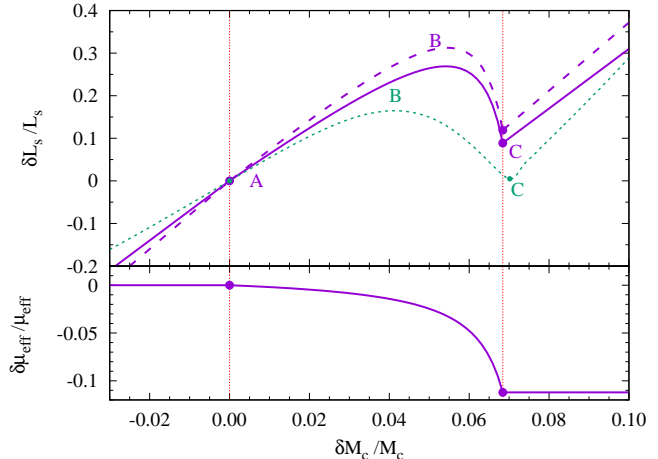


**Figure 5.** Upper panel: The solid curve shows the relative changes in the shell luminosity as a function of the relative changes in the core mass according to eq. 22 ( $\nu = 13$ ). The dashed purple curve shows relative changes in the shell luminosity when  $\nu = 16$  is adopted in the derivation of shell-source homology relations. The green dotted curve shows the evolution of the FEMs presented in Fig. 1. Bottom panel: Relative changes in the effective mean molecular weight assumed in our toy model (eq. 21) as the burning shell approaches the chemical discontinuity. Evolution to the left and to the right of the vertical dashed lines proceeds without changes in the mean molecular weight  $\mu$ , and according to  $\delta L/L = 7\delta M_c/M_c$  for  $\nu = 13$  (solid purple line) and  $\delta L/L = 8\delta M_c/M_c$  for  $\nu = 16$  (dashed purple line).

that includes the connection between the location of the burning shell, the mean molecular weight of the outer mantle and the mass of the core. With the help of this simple model we have shown in Section 3.2 that, when the mean molecular weight drops during the RGBB, the feedback of the temperature of the burning shell on the inner isothermal mantle, leads to a decrease in the radius of the burning shell that attenuates the luminosity drop. When this feedback is taken into account together with the description by Christensen-Dalsgaard (2015), of how the effective mean molecular weight of the outer mantle changes as the burning shell approaches the chemical discontinuity, shell-source homology relations are completely able to quantitatively explain what is observed in FEMs. Specifically, when taking into account the increase of the core mass and the decrease in the effective mean molecular weight as the burning shell approaches the discontinuity, together with feedback of the inner mantle the predictions of shell homology relations are in agreement with FEMs. This definitely clarifies the role played by each part of the star in the formation of the RGBB and how the luminosity changes as the burning shell approaches the chemical discontinuity.

Moreover, in Section 2, we have shown that the theoretical framework developed in Miller Bertolami (2022) can be used to give a more specific meaning to the quantities involved in shell-source homology relations. In particular, this approach clarifies which value of  $\mu$  (i.e. at which point in the star) is relevant for shell-source homology relations.

In addition, we have shown in Section 4 that the whole evolution of the stellar luminosity before and after the RGBB can be described with a simple model that takes into account the previously mentioned feedback and the change in the effective mean molecular weight as the burning shell approaches the discontinuity. Most importantly, this description emphasizes that both the initial slowing down of the luminosity increase (from model A to B, Figs. 1 and 3), and the posterior drop in luminosity (from model B to C, Figs. 1 and 3) all take place on a nuclear timescale (i.e. in thermal equilibrium), as the burning shell burns its way towards the chemical discontinuity left by convection. Consequently, this toy model demonstrates that the luminosity changes during the RGBB are just a consequence of the changes in the temperature of the burning shell produced by variations of the effective mean molecular weight of the outer mantle, and the consequent impact of those tempera-

ture changes in structure of the inner mantle of the red giant (Fig. 2). We believe this toy model has great pedagogical potential for discussing the RGBB.

In closing we would like to mention that the clear description of the RGBB obtained here, from the simple models devised in Christensen-Dalsgaard (2015) and Miller Bertolami (2022), highlights the importance of simple mental models when interpreting and understanding the results from detailed numerical simulations.

## ACKNOWLEDGMENTS

The author thanks the Max Planck Institute for Astrophysics and Achim Weiß for several research stays during which many of the ideas in this work were conceived and developed. The author also thanks Jørgen Christensen-Dalsgaard, Alfred Gautschy, and the anonymous referee for comments and corrections that highlighted shortcomings in the first version of this paper. M3B is partially supported by PIP 2971 from CONICET and PICT 2020-03316 from Agencia I+D+i.

*Software:* LPCODE: Althaus et al. (2003, 2005); Miller Bertolami (2016); Althaus et al. (2020)

## APPENDIX

### A. SHELL-SOURCE HOMOLOGY RELATIONS WITH VARYING $\mu$

Shell-source homology was first introduced by Refsdal & Weigert (1970) and is based on several simplifying assumptions:

1. It is assumed that there exist a region of negligible mass ( $\Delta m \ll M_c$ ) from the bottom of the burning shell ( $r = r_-$ ) to a point  $r = R_0$  above the burning shell ( $R_0 > r_+$ ), where  $T$ ,  $P$ , and  $\rho$  decrease significantly from their values at the burning shell (i.e.  $T(R_0) \ll T_s$ ,  $P(R_0) \ll P_s$ ,  $\rho(R_0) \ll \rho_s$ , and  $l(R_0) = l(r_+) = L_s + L_c$ , where usually  $L_c = 0$ ).
2. That region of the star is assumed in “thermal equilibrium” (i.e.  $dl/dm = \epsilon_n$ ).
3. The gas is considered to be an ideal classical gas  $P = \Re\rho T/\mu$ . Note that Refsdal & Weigert (1970) extends this to a classical gas plus radiation.
4. Heat is transported by radiation in the whole region.
5. Physical quantities in the region of concern ( $r_- < r < R_0$ ) are only sensitive to the radius ( $R_s$ ) and mass of the core ( $M_c$ ), and to a characteristic mean molecular weight of the material in the region ( $\bar{\mu}$ ), in the sense that a set of solutions of the stellar structure equations  $\rho(r)$ ,  $T(r)$ ,  $P(r)$ ,  $l(r)$  (corresponding to  $M_c, R_s, \bar{\mu}$ ) and a set of solutions of the stellar structure equations  $\rho'(r')$ ,  $T'(r')$ ,  $P'(r')$ ,  $l'(r')$  (corresponding to  $M'_c, R'_s, \bar{\mu}'$ ) evaluated at homologous points ( $r/R_s = r'/R'_s$ ) are related by

$$\frac{\rho}{\rho'} = \left(\frac{M_c}{M'_c}\right)^{\varphi_1} \left(\frac{R_s}{R'_s}\right)^{\varphi_2} \left(\frac{\bar{\mu}}{\bar{\mu}'}\right)^{\varphi_3} \quad (\text{A1})$$

$$\frac{T}{T'} = \left(\frac{M_c}{M'_c}\right)^{\psi_1} \left(\frac{R_s}{R'_s}\right)^{\psi_2} \left(\frac{\bar{\mu}}{\bar{\mu}'}\right)^{\psi_3} \quad (\text{A2})$$

$$\frac{P}{P'} = \left(\frac{M_c}{M'_c}\right)^{\tau_1} \left(\frac{R_s}{R'_s}\right)^{\tau_2} \left(\frac{\bar{\mu}}{\bar{\mu}'}\right)^{\tau_3} \quad (\text{A3})$$

$$\frac{l}{l'} = \left(\frac{M_c}{M'_c}\right)^{\sigma_1} \left(\frac{R_s}{R'_s}\right)^{\sigma_2} \left(\frac{\bar{\mu}}{\bar{\mu}'}\right)^{\sigma_3}, \quad (\text{A4})$$

When working with shell-source homology relations it is also typical to assume that the massive envelope is also



in thermal equilibrium and  $L_s = L_*$ , although this is not needed to derive the behavior of the burning shell but to link it to the surface luminosity of the star.

Assuming power laws for the specific energy generation rate  $\epsilon$  and the radiative opacity  $\kappa$  ( $\epsilon \propto \rho^{n-1}T^\nu$  and  $\kappa \propto P^a T^b$ ) it is possible to show that the coefficients in eqs. A1 to A4 fulfill.

$$\begin{aligned} \psi_1 &= 1, & \varphi_1 &= \frac{4 - \nu - a - b}{1 + a + n}, \\ \tau_1 &= \varphi_1 + 1, & \sigma_1 &= \varphi_1 n + \nu, \\ \psi_2 &= -1, & \varphi_2 &= \frac{-6 + \nu + a + b}{1 + a + n}, \\ \tau_2 &= \varphi_2 - 1, & \sigma_2 &= \varphi_2 n - \nu + 3, \\ \psi_3 &= 1, & \varphi_3 &= \frac{4 - \nu - a - b}{1 + a + n}, \\ \tau_3 &= \varphi_3, & \sigma_3 &= \varphi_3 n + \nu. \end{aligned} \quad (\text{A5})$$

A detailed explanation of how to obtain these results can be found in Chapters §33.2 and §33.3 of Kippenhahn et al. (2012), and in the original article by Refsdal & Weigert (1970). As discussed in section 2 the meaning of  $\bar{\mu}$  is not well defined. The most natural way by which one can characterize the chemical composition of the relevant region by only one parameter ( $\bar{\mu}$ )

is by assuming that the function  $\mu(r/R_s)$  is related to  $\mu'(r'/R'_s)$  by a single factor  $\mu(r/R_s)/\mu'(r'/R'_s) = \bar{\mu}/\bar{\mu}'$ . This is not realistic as, at the bottom of the burning shell of two stellar models the mean molecular weight must be that of the core  $\mu(r_-/R_s) = \mu'(r'_-/R'_s) = \mu_c$ . Alternatively, one can assume  $\bar{\mu}$  to represent some ill-defined value of the mean molecular weight of the whole region. As discussed in section 2, the framework developed by Miller Bertolami (2022) shows that  $\bar{\mu}$  is very close to the mean molecular weight immediately above the burning shell ( $\bar{\mu} \simeq \mu_{\text{env}}$ ) with very minor corrections (see eqs. 5 to 8).

For the conditions in red giants, the values of  $a = b = 0$  (Thomson scattering) and  $\nu = 13$ ,  $n = 2$  have been used extensively (Kippenhahn et al. 2012). This implies that the dependence of the shell luminosity is  $L \propto M_c^7 R_c^{-16/3} \bar{\mu}^7$ . Thomson scattering is, in fact, a very good approximation of the conditions at the burning shell in red giants. At the typical lower temperatures of the RGBB ( $T_s \simeq 2.85 \times 10^7 \text{K}$ ) the temperature dependence of the CNO cycle is closer to  $\nu = 16$ . With these choices the dependence of the shell luminosity is  $L \propto M_c^8 R_c^{-19/3} \bar{\mu}^8$ , which gives results closer to the predictions of FEMs.

## REFERENCES

- Althaus, L. G., Córscico, A. H., & De Gerónimo, F. 2020, A&A, 644, A55, doi: [10.1051/0004-6361/202039557](https://doi.org/10.1051/0004-6361/202039557)
- Althaus, L. G., Serenelli, A. M., Córscico, A. H., & Montgomery, M. H. 2003, A&A, 404, 593, doi: [10.1051/0004-6361:20030472](https://doi.org/10.1051/0004-6361:20030472)
- Althaus, L. G., Serenelli, A. M., Panei, J. A., et al. 2005, A&A, 435, 631, doi: [10.1051/0004-6361:20041965](https://doi.org/10.1051/0004-6361:20041965)
- Cassisi, S., Salaris, M., & Bono, G. 2002, ApJ, 565, 1231, doi: [10.1086/324695](https://doi.org/10.1086/324695)
- Christensen-Dalsgaard, J. 2015, MNRAS, 453, 666, doi: [10.1093/mnras/stv1656](https://doi.org/10.1093/mnras/stv1656)
- Gai, N., & Tang, Y. 2015, ApJ, 804, 6, doi: [10.1088/0004-637X/804/1/6](https://doi.org/10.1088/0004-637X/804/1/6)
- Hekker, S., Angelou, G. C., Elsworth, Y., & Basu, S. 2020, MNRAS, 492, 5940, doi: [10.1093/mnras/staa176](https://doi.org/10.1093/mnras/staa176)
- Iben, Icko, J. 1968, ApJ, 154, 581, doi: [10.1086/149782](https://doi.org/10.1086/149782)
- King, C. R., Da Costa, G. S., & Demarque, P. 1985, ApJ, 299, 674, doi: [10.1086/163733](https://doi.org/10.1086/163733)
- Kippenhahn, R., Weigert, A., & Weiss, A. 2012, Stellar Structure and Evolution, doi: [10.1007/978-3-642-30304-3](https://doi.org/10.1007/978-3-642-30304-3)
- Miller Bertolami, M. M. 2016, A&A, 588, A25, doi: [10.1051/0004-6361/201526577](https://doi.org/10.1051/0004-6361/201526577)
- . 2022, ApJ, in press, arXiv:2210.07005, <https://arxiv.org/abs/2210.07005>
- Refsdal, S., & Weigert, A. 1970, A&A, 6, 426
- Sweigart, A. V., Greggio, L., & Renzini, A. 1990, ApJ, 364, 527, doi: [10.1086/169434](https://doi.org/10.1086/169434)
- Thomas, H.-C. 1967, ZA, 67, 420